

1           **A new methodology for measuring traveling quasi-5-day**  
2           **oscillations during SSWs based on satellite observations**

3  
4  
5           Zheng Ma<sup>1,2,3</sup>, Yun Gong<sup>1,2,3</sup>, Shaodong Zhang<sup>1,2,3,4,5</sup>, Qiao Xiao<sup>1,3</sup>,  
6           Chunming Huang<sup>1,2,3</sup>, and Kaiming Huang<sup>1,2,3</sup>

- 7  
8  
9   1. School of Electronic Information, Wuhan University, Wuhan, China.  
10  2. Hubei LuoJia Laboratory, Wuhan, China.  
11  3. Key Laboratory of Geospace Environment and Geodesy, Ministry of Education,  
12    Wuhan, China.  
13  4. State Key Laboratory of Information Engineering in Surveying, Mapping and  
14    Remote Sensing, Wuhan University, Wuhan, China.  
15  5. Guizhou Normal University, Guiyang, China.

16  
17  
18  
19  Correspondence to Yun Gong (yun.gong@whu.edu.cn)  
20

21 **Abstract**

22 Enhancements of stationary planetary waves (SPWs) and traveling planetary  
23 waves (TPWs) are commonly observed in the middle atmosphere during sudden  
24 stratospheric warming (SSW) events. Based on the least-square fitting method (Wu et  
25 al., 1995), numerous studies have used satellite measurements to investigate the  
26 characteristics of TPWs during SSWs but ignored the effect of the SPWs. However, a  
27 rapid and large change in the SPWs during SSWs may lead to significant disturbances  
28 in the amplitude of derived TPWs. In this study, we present a new methodology for  
29 obtaining the amplitudes and wavenumbers of traveling quasi-5-day oscillations  
30 (Q5DOs) in the middle atmosphere during major SSWs. Our new fitting method is  
31 developed by inhibiting the effect of a rapid and large change in SPWs during SSWs.  
32 We demonstrate the effectiveness of the new method using both synthetic data and  
33 satellite observations. The results of the simulations indicate that the new method can  
34 suppress the aliasing from SPWs and capture the real variations of TPWs during SSWs.  
35 Based on the geopotential height data measured by the Aura satellite from 2004 to 2021,  
36 the variations of traveling Q5DOs during eight mid-winter major SSWs are reevaluated  
37 using the new method. The differences in the fitted amplitudes between the least-square  
38 fitting method and the new method are usually over 100 m during the SSW onsets. Our  
39 analysis indicates that previously-reported Q5DOs during SSWs might be  
40 contaminated by SPWs, which leads to both overestimation and underestimation in the  
41 amplitudes of the traveling Q5DOs.

42

## 43 **1. Introduction**

44 Sudden stratospheric warming (SSW) is one of the most representative phenomena  
45 in the atmospheric dynamics in the polar region, which is excited by the interaction  
46 between stationary planetary waves (SPWs) and background mean flow (Matsuno,  
47 1971; Baldwin et al., 2021). The onset of SSW is characterized by a positive gradient  
48 of zonal mean temperature from 90°N to 60°N at 10 hPa (Andrews et al., 1987).  
49 Generally, a major SSW event is additionally associated with the phenomenon of wind  
50 reversals in the zonal mean eastward winds at 60°N and 10 hPa; otherwise, SSWs are  
51 regarded as minor events (Charlton and Polvani, 2007; Butler et al., 2017; Choi et al.,  
52 2019). During the occurrence of SSWs, the enhancements of SPWs largely affect the  
53 energy transportation in the stratosphere and the occurrence of extreme weather in the  
54 troposphere at middle latitudes (e.g., Manney et al., 2009; Kozubek et al., 2015; King  
55 et al., 2019; Domeisen et al., 2020). The zonal wavenumber of the enhanced SPWs  
56 usually corresponds to the geometry of the polar vortex during SSWs (e.g., Harada and  
57 Hirooka, 2017; Liu et al., 2019; White et al., 2021). A displacement vortex is mainly  
58 due to a strong SPW with a zonal wavenumber of 1 (SPW1) and split vortices are  
59 always associated with large SPWs with a zonal wavenumber of 2 (SPW2) (e.g.,  
60 Seviour et al., 2013; Lawrence and Manney, 2018; Choi et al., 2019).

61 Traveling planetary waves (TPWs), widely observed with strong amplitudes  
62 during SSWs in recent decades, also play a significant role in controlling the global  
63 atmospheric and ionospheric couplings during SSWs (e.g., Gong et al., 2019; Koushik  
64 et al., 2020; Lin et al., 2020; Ma et al., 2022). One of the prominent TPWs, the westward

65 propagating quasi-5-day oscillation (Q5DO) with periods of 4-7 days, is usually  
66 observed from the mesosphere to the ionosphere at mid-latitudes during SSWs with the  
67 zonal wavenumbers both 1 and 2 (W1 and W2) (Gong et al., 2018; Pancheva et al.,  
68 2018; Yamazaki et al., 2020, 2021). These Q5DOs are believed to be generated by  
69 atmospheric barotropic/baroclinic instability due to large changes in zonal winds and  
70 temperatures during SSWs (e.g., Liu et al., 2004; Ma et al., 2020; Yamazaki et al., 2021).  
71 Based on the least-square fitting method introduced by Wu et al. (1995), the amplitude,  
72 phase, and zonal wavenumber of the Q5DOs can be obtained from satellite observations  
73 and reanalysis data sets (e.g., Huang et al., 2017; Qin et al., 2021). However, based on  
74 the least-square fitting method, a rapid and large change in the amplitudes of SPWs  
75 would lead to an apparent fluctuation in the amplitude of TPWs over a broad range of  
76 frequencies, including those corresponding to Q5DOs. Yamazaki and Matthias (2019)  
77 proposed that based on the least-square fitting method, the effect of an SPW on a quasi-  
78 10-day wave (Q10DW) is equivalent to two oppositely propagating waves with equal  
79 amplitudes, periods, and wavenumbers. They suggested that the effect of SPWs can be  
80 ignored when the activities of Q10DWs in the oppositely propagating direction were  
81 not simultaneously enhanced.

82       However, the rapid change in the amplitudes of SPWs is a typical characteristic  
83 during the occurrence of SSWs. Previous studies usually ignored the effect of SPWs  
84 when obtaining the amplitudes of Q5DOs from satellite observations (e.g., Gong et al.,  
85 2018; Qin et al., 2021). Nevertheless, both westward and eastward Q5DOs have been  
86 frequently reported during SSWs in recent years (e.g., Pancheva et al., 2018; Rhodes et

87 al., 2021; Wang et al., 2021; Yu et al., 2022). Thus, it is necessary to understand the real  
88 physics of the enhanced Q5DOs during SSWs and their relationships with SPWs. It is  
89 also necessary to inhibit the effect of SPWs when studying the variations of Q5DOs  
90 during SSWs. In the present study, we develop a new method for measuring the  
91 variation of westward and eastward propagating Q5DOs by inhibiting the effect of a  
92 rapid and large change in SPWs. The effectiveness of the new method is demonstrated  
93 by using both synthetic data and satellite observations. The paper is organized as  
94 follows. In Section 2, the synthetic data and the satellite data used in this study are  
95 introduced. Section 3 presents the new methodology for measuring the amplitudes of  
96 Q5DOs. Discussions are given in Section 4, mainly focusing on the comparisons of  
97 traveling Q5DOs during SSWs between the least-square fitting method and the new  
98 fitting method. Conclusions are summarized in section 5.

## 99 **2. Data**

100 In the present study, an experiment is performed based on synthetic data to further  
101 understand the issue of SPWs and Q5DOs during SSWs. The synthetic data  $Y(x, t)$   
102 are built based on equation (1), including three components: an SPW, a westward  
103 propagating Q5DO, and an eastward propagating Q5DO, respectively, which is  
104 expressed as:

$$105 Y(x, t) = A_k(t) \cos(kx - \varphi_k) + B_w \cos(\omega t + kx - \varphi_w) + B_e \cos(\omega t - kx - \varphi_e) \quad (1)$$

106 where  $x$  is the longitudes,  $t$  is the time,  $k$  is the wavenumber,  $\omega$  is the frequency of  
107 Q5DOs,  $A_k$  and  $\varphi_k$  are the amplitude and phase of SPWs,  $B_w$  and  $B_e$  denote the

108 amplitudes of westward and eastward Q5DOs with the phase of  $\varphi_w$  and  $\varphi_e$ ,  
109 respectively. Based on the least-square fitting method introduced by Wu et al. (1995),  
110 TPWs with the same zonal wavenumber but in other periods only cause periodic  
111 modulation in the fitted amplitudes of Q5DOs. The aliasing caused by TPWs with  
112 different wavenumbers is mainly captured in the studies of quasi-2-day waves based on  
113 satellite measurements (Tunbridge et al., 2011). For the analysis of Q5DOs, the aliasing  
114 due to components with different wavenumbers is usually ignored, because Q5DOs  
115 with wavenumbers of 3 or 4 are rarely reported. Nevertheless, the most important issue  
116 of the least-square fitting method may be the aliasing due to the rapid and large changes  
117 in the SPWs. Therefore, to better understand the issue, the synthetic data for the  
118 simulations in the present study only includes three components of waves with the same  
119 zonal wavenumbers.

120 To verify the effectiveness of different fitting methods, the geopotential height data  
121 measured by the Aura/Microwave Limb Sounder (MLS) from 2005 to 2021 are used to  
122 derive the Q5DOs in the present study. The available Aura/MLS geopotential height  
123 data in the version 4.2x Level 2 product is from 261 hPa to 0.001 hPa (Livesey et al.,  
124 2017), with the measurement errors of  $\pm 25$  m,  $\pm 45$  m,  $\pm 110$  m, and  $\pm 160$  m at 1 hPa,  
125 0.1 hPa, 0.01 hPa, and 0.001 hPa. A comprehensive study of the measurement errors  
126 and fitting errors has been reported by Yamazaki and Matthias (2019) when using the  
127 Aura/MLS geopotential height data to obtain the amplitudes of Q5DOs. They have  
128 suggested that the mean values of the estimated  $1-\sigma$  uncertainties in TPWs are about 50  
129 m at high latitudes in the Northern Hemisphere. Following their technique, mean values

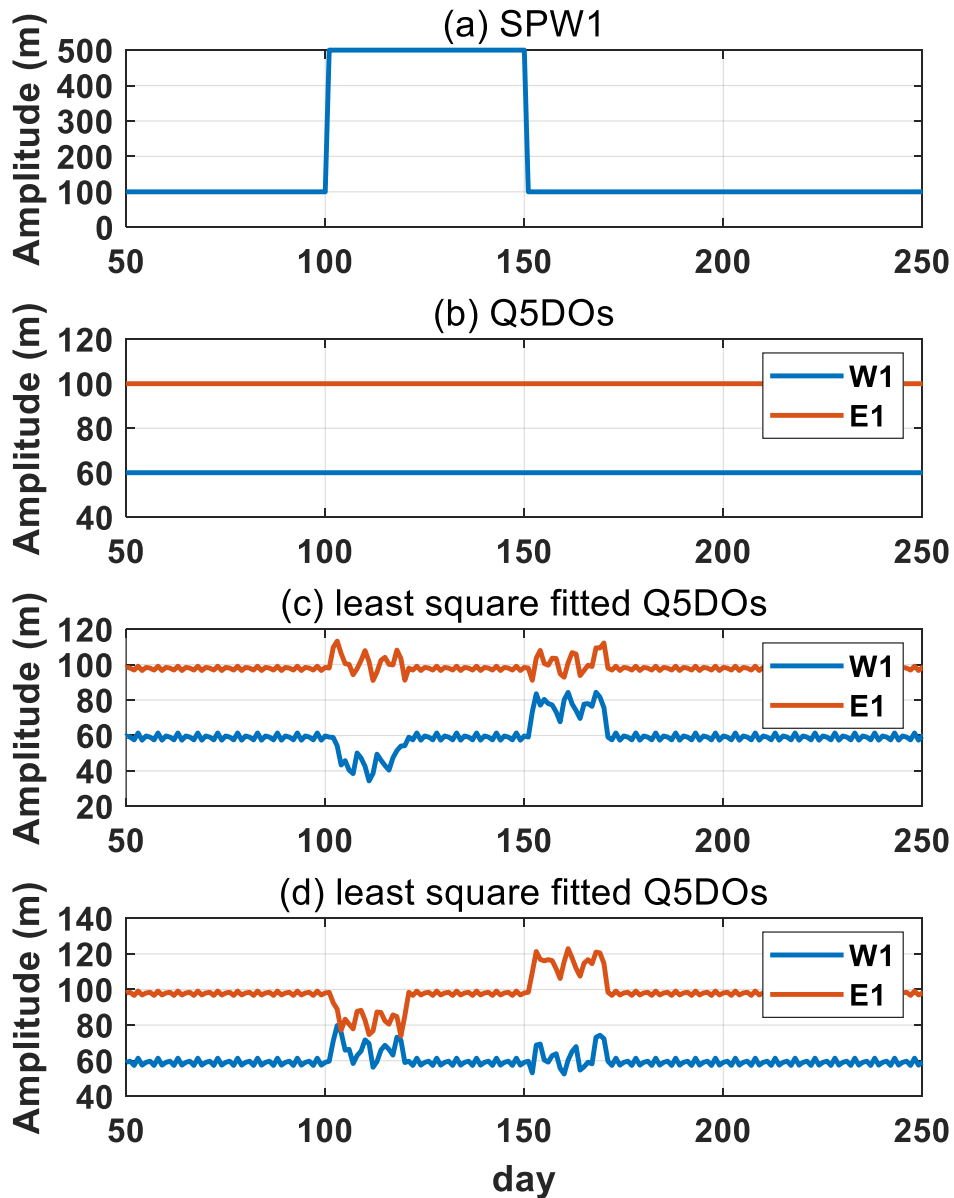
130 of the estimated  $1\text{-}\sigma$  uncertainties in the fitted amplitudes obtained by the new method  
131 are also about 50 m. The vertical structure of the estimated  $1\text{-}\sigma$  uncertainty of the new  
132 method is the same as the distributions shown in Figure 1 of Yamazaki and Matthias  
133 (2019). In the present study, we focus on the difference between the original and new  
134 fitting methods. The fitted amplitudes are presented in the following analyses without  
135 dropping the values that are lower than the uncertainties. The analysis of this study  
136 focuses on the traveling Q5DOs with zonal wavenumbers of 1 and 2 based on the data  
137 at  $60^\circ\text{N}$  (averaged from  $55\text{-}65^\circ\text{N}$ ).

### 138 **3. Methodology**

#### 139 **3.1 Simulations of the least-square fitting method**

140 The least-square fitting method used in previous studies to derive the amplitude  
141 and phase of Q5DOs from satellite observations is based on equation (1) but without  
142 fitting the first term on the right-hand side (e.g., Huang et al., 2017; Qin et al., 2021).  
143 Generally, a 20-day sliding window with a step of one day is used to simultaneously  
144 extract the amplitudes of TPWs with zonal wavenumbers from 3 to -3 (westward to  
145 eastward). The daily amplitudes of the Q5DOs are obtained with the largest value in  
146 the wave periods between 4 and 7 days. The fitting result is marked at the end day of  
147 each 20-day window. To better understand the original least-square fitting method, the  
148 synthetic data are used to first simulate the effect of a rapid and large change in SPWs  
149 when calculating the amplitudes of Q5DOs. As shown in Figures 1a and 1b, three  
150 components of waves with the zonal wavenumber of 1 are given in the synthetic data,

151 which are an SPW with the amplitude of 100 m, eastward and westward propagating  
 152 Q5DOs with amplitudes of 100 m and 60 m, respectively. The phases are respectively  
 153 set as  $0$ ,  $-\pi/4$ , and  $\pi/5$  for the SPW and the westward and eastward propagating Q5DOs.  
 154 To simulate the effect of SPWs on TPWs, rapid large changes are given in the  
 155 amplitudes of SPW on day 100 with magnitudes from 100 m to 500 m and on day 150  
 156 with magnitudes from 500 m to 100 m (see Figure 1a).



157



158 Figure 1. Simulations of the least-square fitting method based on synthetic data, which  
159 includes an SPW and westward and eastward Q5DOs with zonal wavenumber of 1. (a)  
160 Daily variations of the SPW amplitudes. The phase of the SPW is 0. (b) The real  
161 amplitudes of Q5DOs. Amplitudes are separately set as 100 m and 60 m for the  
162 eastward and westward Q5DOs. (c) Q5DOs obtained from the least-square fitting  
163 method. The phases are  $-\pi/4$  and  $\pi/5$  for the westward and eastward Q5DOs,  
164 respectively. (d) Same as (c) but with phases of  $\pi/4$  and  $-\pi/5$  for the westward and  
165 eastward Q5DOs.

166 Figure 1c presents the amplitudes of the westward and eastward propagating  
167 Q5DOs fitted by the least-square fitting method. As shown in Figure 1c, abnormal  
168 fluctuations after day 100 and day 150 are captured, which correspond to the occurrence  
169 of rapid large changes in the amplitudes of SPW. However, Figure 1c suggests that the  
170 fitted Q5DOs are not largely influenced by the SPWs when rapid large changes are not  
171 given in the amplitudes of SPWs (before day 100 or from day 120 to 150). Additionally,  
172 Figure 1c indicates that abnormal fluctuations in Q5DOs induced by SPWs are not  
173 equivalent to two oppositely propagating directions. An enhancement and a decrease in  
174 the amplitudes of westward and eastward propagating Q5DOs can be simultaneously  
175 observed. Results shown in Figure 1d are the same as that in Figure 1c but are derived  
176 based on different phases of the westward and eastward Q5DOs in the synthetic data,  
177 where  $\pi/4$ , and  $-\pi/5$  are given in the westward and eastward Q5DOs. Comparing the  
178 results between Figures 1c and 1d, it is interesting to note that the effect of a rapid large  
179 change in SPWs on the derived Q5DOs also depends on the phase relationships.

180 Yamazaki and Matthias (2019) suggested that the effect of SPWs could be ignored when  
 181 the activities of Q10DWs in the oppositely propagating direction were not  
 182 simultaneously enhanced. However, according to our simulations, this criterion is not  
 183 suitable for the analysis of Q5DOs with different phases. Our simulation indicates that  
 184 the influence of a quick and large change of SPW should not be ignored when extracting  
 185 Q5DOs during SSWs from satellite observations based on the least-square fitting  
 186 method. Thus, in this study, we develop a new fitting method to derive the Q5DOs by  
 187 suppressing the effect of a rapid and large change in SPWs.

### 188 **3.2 New fitting method**

189 Since the daily amplitude of SPW ( $A_k(t)$ ) cannot be directly derived when  
 190 Q5DOs exist, the primary goal of the new method is to eliminate the rapid and large  
 191 changes in  $A_k(t)$ . The following steps are performed, where SPWs and Q5DOs are  
 192 considered within the same wavenumbers.

#### 193 **Step 1. Estimate the daily variations of SPWs.**

194 Based on the definition of SPW, the phase  $\varphi_k$  should be a fixed value in each  
 195 window. Therefore,  $\varphi_k$  is first fitted based on  $y(x) = a_k \cos(kx - \varphi_k)$ , where  $y(x)$   
 196 is the time-averaged geopotential height in each 20-day window. Using the fitted phase  
 197  $\varphi_k$ , the daily amplitudes of SPW can be roughly estimated by the least-square fitting  
 198 based on equation (2), which equals equation (1).

$$\begin{aligned}
 199 \quad Y(x, t) = & [A_k(t) + B_w \cos(\omega t - \varphi_w + \varphi_k) + B_e \cos(\omega t - \varphi_e - \varphi_k)] \cos(kx - \varphi_k) \\
 200 \quad & + [B_e \sin(\omega t - \varphi_e - \varphi_k) - B_w \sin(\omega t - \varphi_w + \varphi_k)] \sin(kx - \varphi_k) \quad (2)
 \end{aligned}$$

201 If we let  $a_k(t) = A_k(t) + B_w \cos(\omega t - \varphi_w + \varphi_k) + B_e \cos(\omega t - \varphi_e - \varphi_k)$ , and

202  $b_k(t) = B_e \sin(\omega t - \varphi_e - \varphi_k) - B_w \sin(\omega t - \varphi_w + \varphi_k)$ , equation (2) can be simply  
 203 expressed as equation (3):

$$204 \quad Y(x, t) = a_k(t) \cos(kx - \varphi_k) + b_k(t) \sin(kx - \varphi_k) \quad (3)$$

205 However, the fitted amplitudes of SPWs,  $a_k(t)$ , are not the true amplitudes of SPWs  
 206 ( $A_k(t)$ ), which includes the aliasing from Q5DOs. According to the above two  
 207 equations, rapid and large changes in SPW amplitudes can only have impacts on the  
 208 values of  $a_k(t)$ . Because the true values of  $A_k(t)$  cannot be directly fitted due to the  
 209 aliasing of Q5DOs, our goal in Step 2 is to eliminate the rapid large changes in  $a_k(t)$ .

210 **Step 2. Eliminate the large rapid changes in SPWs.**

211 If we let  $P_k(t) = B_w \cos(\omega t - \varphi_w + \varphi_k) + B_e \cos(\omega t - \varphi_e - \varphi_k) =$   
 212  $P \cos(\omega t - \varphi)$ ,  $a_k(t)$  in Equation (3) can be also expressed as,

$$213 \quad a_k(t) = A_k(t) + P_k(t) = A_k(t) + P \cos(\omega t - \varphi) \quad (4)$$

214 The amplitude  $P$  and phase  $\varphi$  can be estimated by the least-square fitting via  
 215 equation (4). Taking the partial derivatives in time on both sides of equation (4), we  
 216 obtain equation (5):

$$217 \quad \frac{\partial}{\partial t} a_k(t) = \frac{\partial}{\partial t} A_k(t) + \frac{\partial}{\partial t} P_k(t) \quad (5)$$

218 where  $\frac{\partial}{\partial t} A_k(t)$  are the daily variations in the amplitudes of SPW. The primary goal of  
 219 Step 2 is to subtract large values of  $\frac{\partial}{\partial t} A_k(t)$  from  $a_k(t)$  to eliminate the large  
 220 variations in  $a_k(t)$ . However,  $\frac{\partial}{\partial t} A_k(t)$  cannot be obtained simply by  $\frac{\partial}{\partial t} A_k(t) =$   
 221  $\frac{\partial}{\partial t} a_k(t) - \frac{\partial}{\partial t} P_k(t)$ , because  $\frac{\partial}{\partial t} P_k(t)$  cannot be derived accurately when  $\left| \frac{\partial}{\partial t} A_k(t) \right|$   
 222 are large (“ $| \quad |$ ” represents the absolute values). Nevertheless, the lower boundary of  
 223 the values in  $\left| \frac{\partial}{\partial t} a_k(t) \right|$  can be estimated when rapid large changes exist in SPWs

224  $\left| \frac{\partial}{\partial t} A_k(t) \right|$  are large). The maximum value in  $\left| \frac{\partial}{\partial t} a_k(t) \right|$  will be at least larger than the  
 225 maximum value in  $\frac{\partial}{\partial t} P_k(t) = -\omega P \sin(\omega t - \varphi)$ , which is  $\omega P$ . Thus, the value of  $\omega P$   
 226 can be used as a threshold to determine rapid large changes in SPWs.

227 Therefore, when  $\left| \frac{\partial}{\partial t} a_k(t) \right|$  are larger than the threshold of  $\omega P$ , we subtract the  
 228 value of the corresponding  $\frac{\partial}{\partial t} A_k(t)$  from all the following members of  $a_k(t)$  to  
 229 obtain a new series of  $a_k^{new}(t)$ . The  $\frac{\partial}{\partial t} A_k(t)$  are estimated by  $\frac{\partial}{\partial t} A_k^{estimated}(t) =$   
 230  $\frac{\partial}{\partial t} a_k(t) - \frac{\partial}{\partial t} P_k^{estimated}(t)$ , where  $P_k^{estimated}(t) = P_{pre} \cos(\omega(t + 1) - \varphi_{pre})$ .  
 231 Instead of the  $P$  and  $\varphi$  fitted in the present window, the  $P_{pre}$  and  $\varphi_{pre}$  fitted from  
 232 the previous one are used because the fitted  $P_{pre}$  and  $\varphi_{pre}$  are not influenced by the  
 233 effect of rapid large changes in SPWs in the present window. Here, we have a new  
 234 series of  $a_k^{new}(t)$  without rapid large changes in SPWs, as well as new fitted  $P$  and  
 235  $\varphi$  for the next window.

### 236 **Step 3. Fit the real amplitudes of Q5DOs.**

237 After obtained the  $a_k^{new}(t)$  and  $b_k(t)$  from Step 2, the reconstruction of the  
 238 original data  $Y'(x, t)$ , which inhibits the rapid and large changes in SPWs, can be  
 239 reconstructed based on equation (6):

$$240 \quad Y'(x, t) = a_k^{new}(t) \cos(kx - \varphi_k) + b_k(t) \sin(kx - \varphi_k) \quad (6)$$

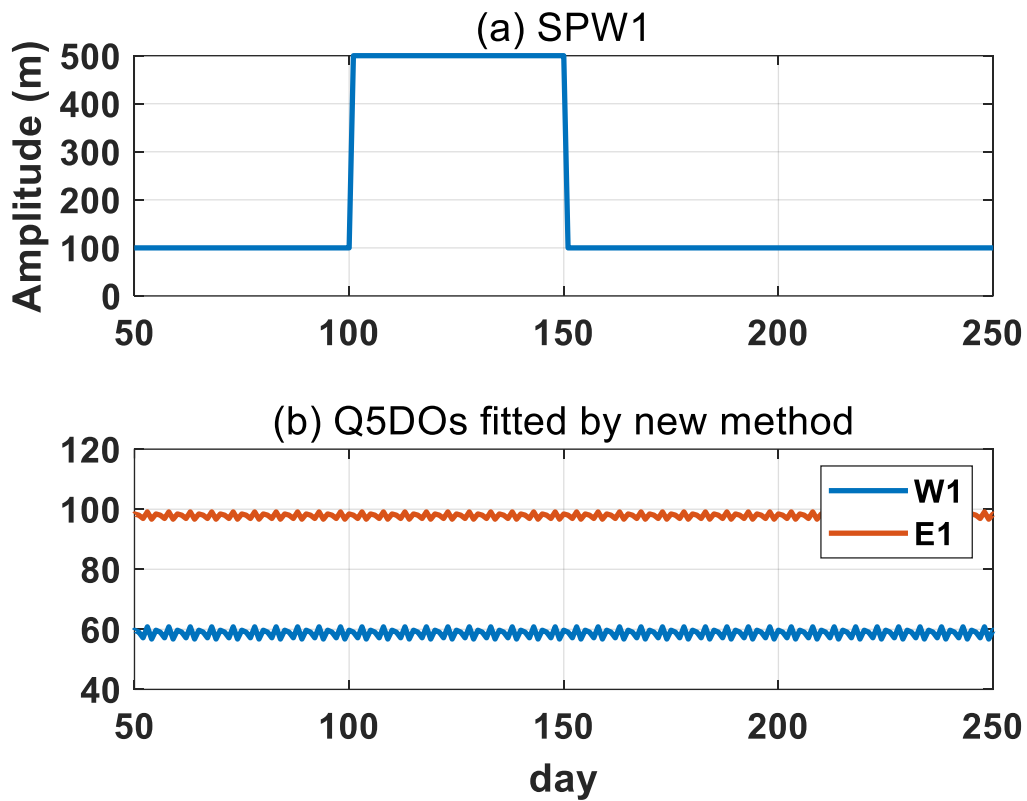
241 Then, the real amplitudes and phases of the Q5DOs ( $B_w$ ,  $B_e$ ,  $\varphi_w$ , and  $\varphi_e$ ) can be fitted  
 242 using the least-square fitting method via  $Y'(x, t) = B_w \cos(\omega t + kx -$   
 243  $\varphi_w) + B_e \cos(\omega t - kx - \varphi_e) + C$ , where  $C$  is a constant.

244 Note that, the effect of small changes in SPWs cannot be eliminated sometimes  
 245 when  $\left| \frac{\partial}{\partial t} a_k(t) \right|$  are smaller than  $\omega P$ . These small changes in SPWs do not have

246 significant effects on the fitted Q5DOs and their elimination depends on the phase  
 247 relationships between westward and eastward Q5DOs. Nevertheless, the Monte Carlo  
 248 simulations based on random phases of Q5DOs reveal that the fake fluctuations in  
 249 Q5DO amplitudes due to this effect will not exceed the value of  $0.1\omega P$ .

## 250 4. Results and Discussions

### 251 4.1 Simulations

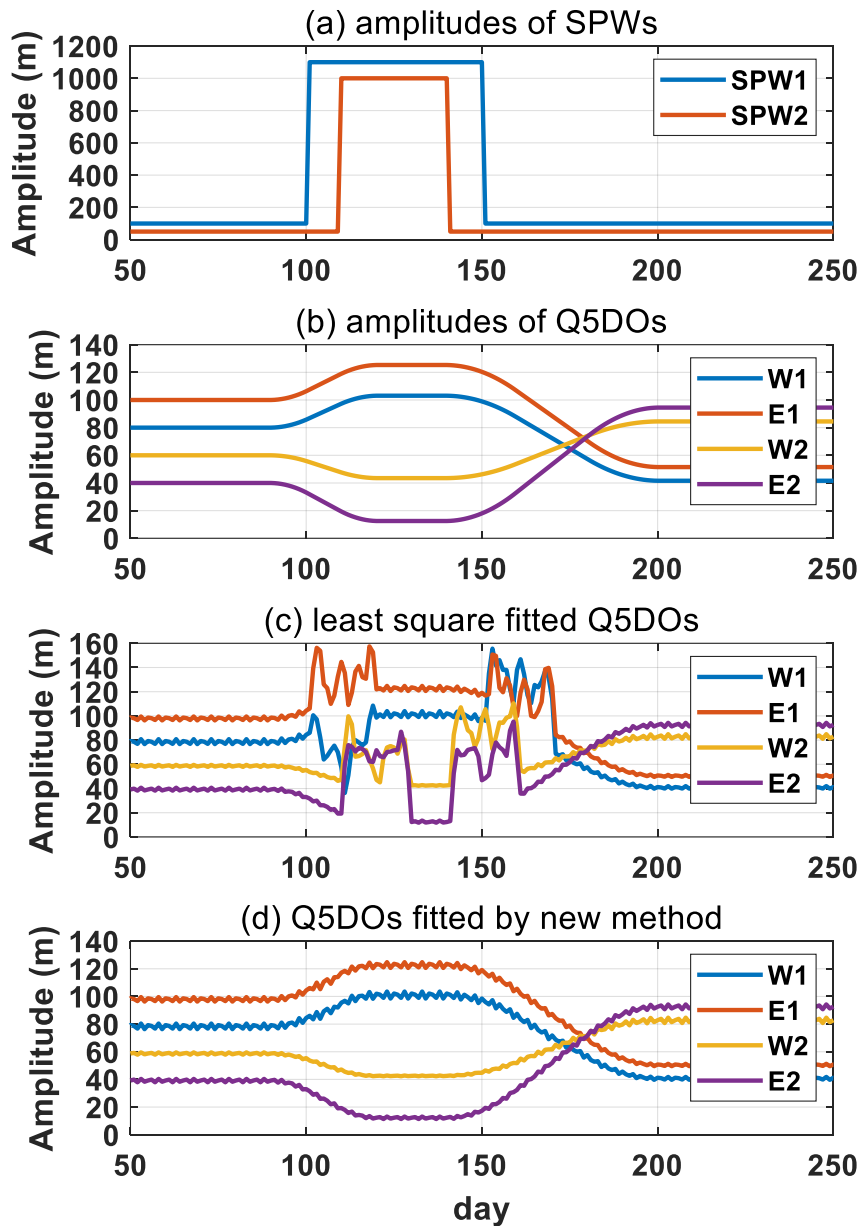


252

253 Figure 2. Simulations of the new fitting method based on synthetic data, which includes  
 254 an SPW and westward and eastward Q5DOs with zonal wavenumber of 1. (a) Daily  
 255 variations of the SPW amplitudes. The phase of the SPW is 0. (b) Q5DOs obtained from  
 256 the new fitting method. The amplitudes are 60 m and 100 m, the phases are  $-\pi/4$  and  
 257  $\pi/5$  for the westward and eastward Q5DOs, respectively.

258 Based on the new fitting method, we present the fitting result in Figure 2. As shown  
259 in Figure 2b, the fitted amplitudes of the Q5DOs are generally consistent with the  
260 amplitudes given in the original synthetic data. The apparent fluctuations in Q5DOs  
261 induced by SPWs have been removed. Note that based on the new fitting method, the  
262 fitted amplitudes are not dependent on the phases of Q5DOs. The new fitting method  
263 will provide the same results as those shown in Figure 2b when Q5DOs have different  
264 phases (not shown). Thus, the fitted amplitudes from the new method do not rely on the  
265 phase relationships of those waves. Figure 2 demonstrates that the new method is  
266 effective to suppress the effect of large rapid change in SPWs, while a further  
267 experiment that synthetic data containing the enhancement of both SPWs and Q5DOs  
268 is needed to demonstrate that the new method can properly capture the changes of  
269 Q5DOs during SSWs. Besides, we also add signals of SPWs and Q5DOs with  
270 wavenumber 2 in the synthetic data to approach the real situation in satellite  
271 observations. Figure 3 shows the results of the further experiment. The synthetic data  
272 used in Figure 3 consist of six components: SPWs with wavenumber 1 and 2 (SPW1  
273 and SPW2), westward propagating Q5DOs with wavenumber 1 and 2 (W1 and W2),  
274 and eastward propagating Q5DOs with wavenumber 1 and 2 (E1 and E2). The daily  
275 variation of the amplitudes for SPWs and Q5DOs are separately shown in Figures 3a  
276 and 3b. The phase of SPW1, SPW2, and W1, E1, W2, and E2 Q5DOs are respectively  
277 set as  $0$ ,  $\pi/6$ ,  $-\pi/4$ ,  $\pi/5$ ,  $-\pi/4$ , and  $\pi/3$ . Figures 3c and 3d present the fitting results for the  
278 least-square fitting method and the new fitting method. As shown in Figure 3d, the  
279 result manifests that the variations of Q5DOs can be captured based on the new method

280 and the effect of large rapid change in SPWs can be limited.



281

282 Figure 3. Simulations of the new fitting method based on synthetic data, which include

283 (a) SPW1 and SPW2 and (b) westward and eastward Q5DOs with zonal wavenumber

284 of 1 and 2. The phase of SPW1, SPW2, and W1, E1, W2, and E2 Q5DOs are

285 respectively set as  $0$ ,  $\pi/6$ ,  $-\pi/4$ ,  $\pi/5$ ,  $-\pi/4$ , and  $\pi/3$ . (c) Daily amplitudes of the fitted

286 Q5DOs obtained from the original least-square fitting method. (d) Daily amplitudes of

287 the fitted Q5DOs obtained from the new fitting method.

288 Note that some sawtooth-shaped points can be seen in the fitting results in Figures  
289 1, 2, and 3. The sawtooth-shaped points are caused by removing the linear declination  
290 on the time series. This process is required in both original and new methods to  
291 eliminate the effect of seasonal trends in the observational data on the fitting of Q5DOs.  
292 The sawtooth-shaped points can be eliminated in the simulation by not removing the  
293 seasonal trends, but we keep them in both original and new methods in the simulations  
294 in order to be consistent with the processes in dealing with the observational data.

## 295 **4.2 Observations**

296 The SPWs and TPWs can be both captured in the mesosphere region and their  
297 origins have been reported in some previous studies. The mesospheric SPWs are usually  
298 believed to be related to the upward wave signals from the troposphere and the lower  
299 stratosphere which rely on the structure of the polar vortex (e.g., Harvey et al., 2018).  
300 In addition, wave-wave interactions, gravity wave forcing, and auroral heating can also  
301 generate mesospheric SPWs (e.g., Lu et al., 2018; Xu et al., 2013; Smith, 2003). The  
302 mesospheric TPWs are generally considered as the result of atmospheric instabilities  
303 and many recent studies have noticed the relationship between extremely strong TPWs  
304 and SSW events (Liu et al., 2004; Ma et al., 2020; Yamazaki et al., 2021). The  
305 mesospheric TPWs during SSWs can be also secondarily generated in situ by wave-  
306 wave interactions (e.g., Xiong et al., 2018; Wang et al., 2021). Nevertheless, the trigger  
307 mechanisms of mesospheric TPWs are still not fully understood due to a lack of long-  
308 term and high-resolution observational data in this region. Thus, satellite observations



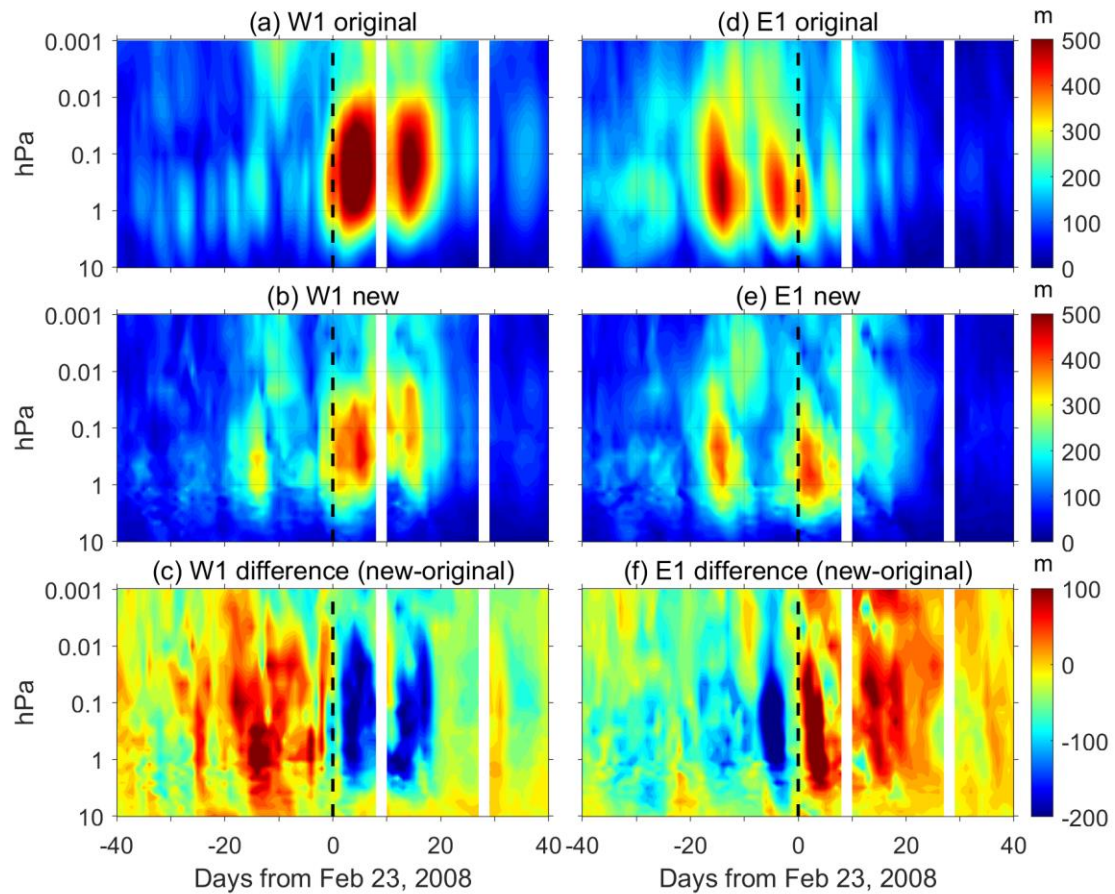
309 are widely used to reveal the feature of mesospheric TPWs. However, as indicated by  
310 our simulations, the previous studies have ignored the effect of rapid and large changed  
311 SPWs when calculating the variations of TPWs during SSWs. Using the geopotential  
312 height data provided by the Aura/MLS measurement, we extract the variations of the  
313 traveling Q5DOs at 60°N during Arctic SSWs. The effectiveness of the new fitting  
314 method is discussed by comparing the results between the original least-square fitting  
315 method and the new method. The daily amplitudes of the Q5DOs are obtained with the  
316 largest value in the wave periods between 4 and 7 days. The fitting result is marked at  
317 the end day of each 20-day window. The traveling Q5DOs with wavenumber 3 and the  
318 amplitudes below 10 hPa are not shown due to their weak amplitudes. In the present  
319 study, the pressure regions from 10 hPa to 1 hPa, from 1 hPa to 0.01 hPa, and from 0.01  
320 hPa to 0.001 hPa are respectively discussed as the stratosphere, mesosphere, and lower  
321 thermosphere.

322         Since the observation of the Aura satellite is available after August 2004, the  
323 variations of traveling Q5DOs are investigated during eight mid-winter major SSWs  
324 from 2005 to 2021 in the present study. Table 1 presents the eight mid-winter major  
325 SSWs with their onset dates. The date with the maximum positive temperature gradient  
326 between 90°N and 60°N at 10 hPa is defined as the SSW onset date, which is obtained  
327 around the date of the first wind reversal during each major event (e.g., Andrews et al.,  
328 1987). Note that the onset date used in the present study is only to roughly determine  
329 the commencement of SSWs and our discussions are not sensitive to the non-uniformed  
330 definitions of SSW onsets (e.g., Butler et al., 2015). In the present study, the SSW in

331 the winter of 2009/2010 is classified as a minor one, because the wind reversal occurred  
332 18 days after the onset date. To be distinguished from the SSW in February 2018, the  
333 SSW with the onset date of December 28, 2018, is discussed as the “2019 SSW” in this  
334 study. The SSWs before 2013 have been widely studied in previous studies (e.g., Choi  
335 et al., 2019; Charlton and Polvani, 2007; Butler et al., 2017; Liu et al., 2019; Rao et al.,  
336 2019), details of the three major SSWs from 2018 to 2021 can be referred to many  
337 recent reports (e.g., Rao et al., 2018, 2020, 2021; Wang et al., 2019; Davis et al., 2022;  
338 Okui et al., 2021; Wright et al., 2021).

339 Table 1. Mid-winter major SSWs from 2005 to 2021.

SSW	Onset Date	First Wind Reversal Date
2006	January 22, 2006	January 21, 2006
2007	February 24, 2007	February 24, 2007
2008	February 23, 2008	February 22, 2008
2009	January 23, 2009	January 24, 2009
2013	January 6, 2013	January 6, 2013
2018	February 11, 2018	February 12, 2018
2019	December 28, 2018	January 2, 2019
2021	January 4, 2021	January 5, 2021

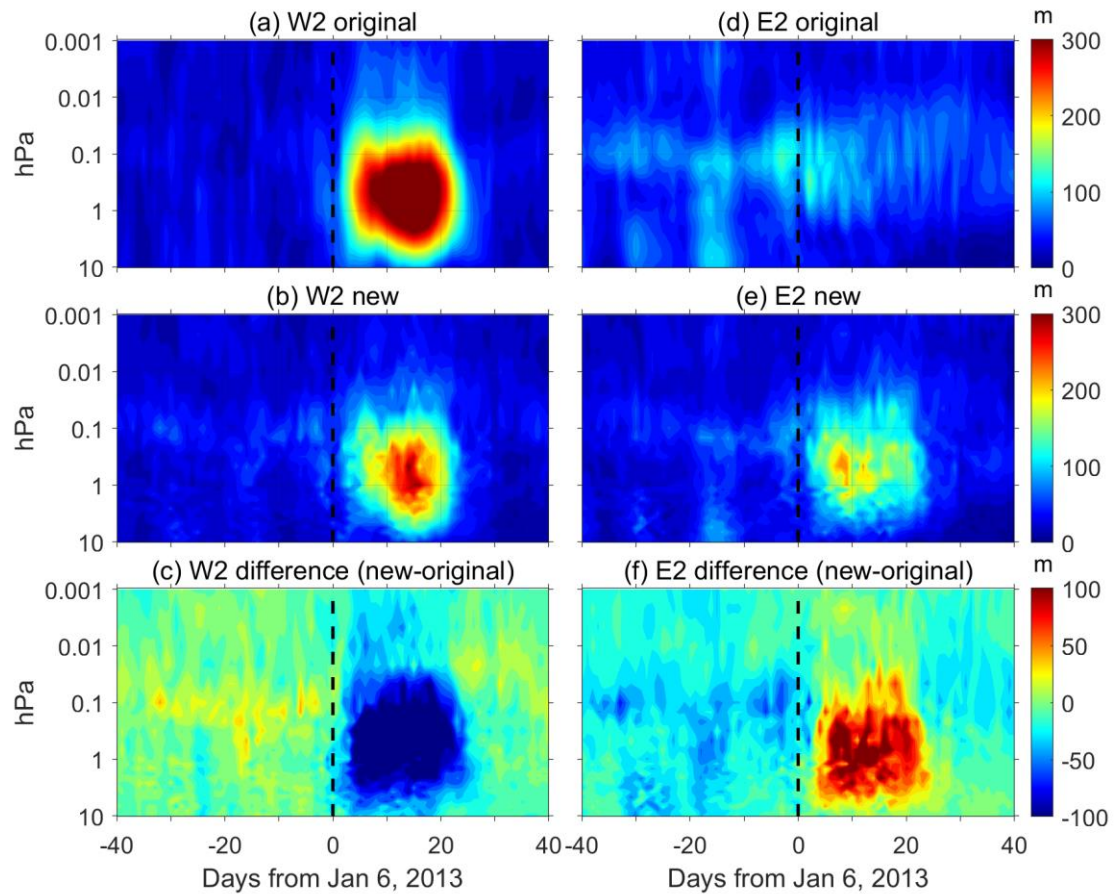


340

341 Figure 4. The amplitudes of W1 (left column) and E1 (right column) Q5DOs during the  
 342 2008 SSW obtained by the original least-square fitting method (top row) and the new  
 343 fitting method (middle row). The differences between the new and original methods are  
 344 shown in the bottom row (c and f). Contour steps are 10 m.

345 Comparisons of fitted amplitudes of traveling Q5DOs are first shown in Figures 4  
 346 and 5, respectively for wavenumber 1 during the 2008 SSW and wavenumber 2 during  
 347 the 2013 SSW. Results for each case are given in 81 days, which is from 40 days before  
 348 to 40 days after the SSW onset date (day 0). Figure 4 presents the amplitudes of W1  
 349 and E1 Q5DOs obtained from both original (top) and new (middle) methods during the  
 350 2008 SSW. The differences are calculated by subtracting the fitting result of the original  
 351 method from the new method, which are given at the bottom of Figure 4. Amplitudes

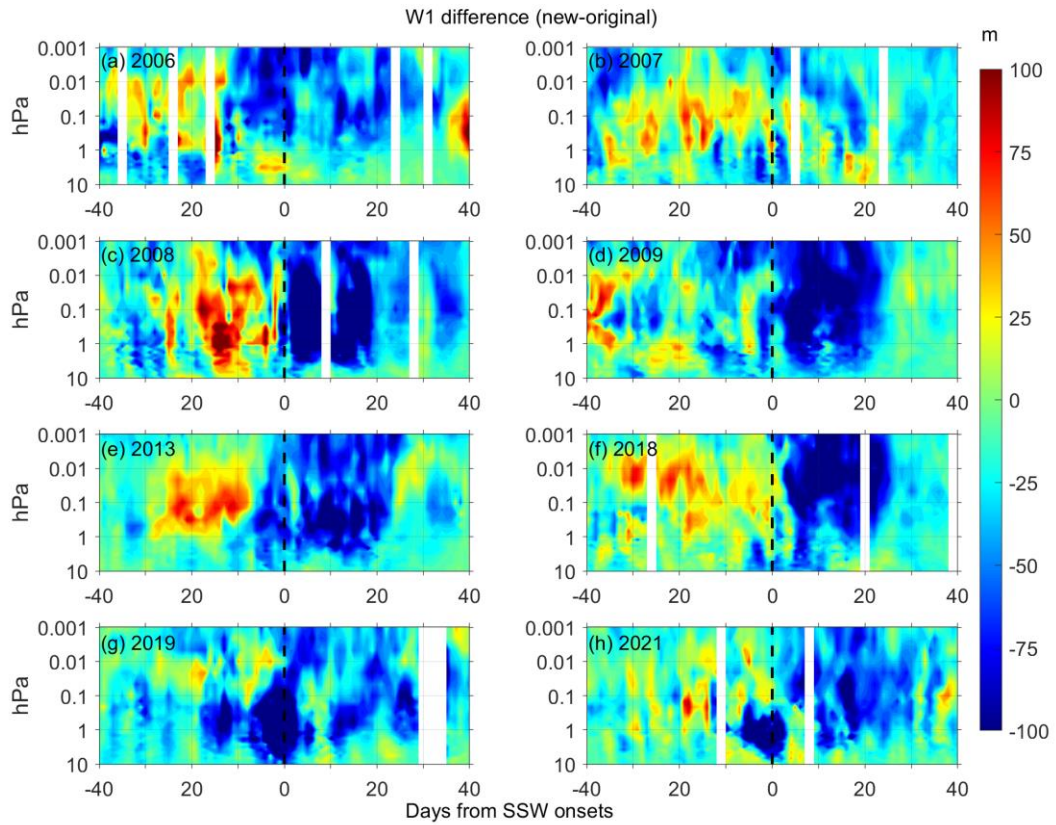
352 are not fitted in the white area where the available data are less than 60% in each  
353 window. As shown in Figure 4a, the W1 Q5DOs fitted by the original least-square  
354 fitting method reveal a significant response to the onset of 2008 SSW. The amplitudes  
355 of the W1 Q5DOs in the mesosphere are larger than 500 m from day 0 to day 20 with  
356 a maximum amplitude of 628 m on day 5. Figure 4b suggests that the amplitudes  
357 obtained from the new method are lower than 500 m during the 2008 SSW. The  
358 maximum amplitude obtained from the new method is 466 m on day 5, which is about  
359 75% of the amplitude obtained from the original least-square fitting method. The  
360 negative differences shown in Figure 4c are generally larger than 200 m from day 0 to  
361 day 20 in the mesosphere, which indicates that the amplitudes of W1 Q5DOs after the  
362 onset of 2008 SSW might be overestimated by the original least-square fitting method.  
363 Nevertheless, positive differences larger than 100 m are also captured before the SSW  
364 onset (day -15) around 1 hPa as shown in Figure 4c, which reveals that the amplitudes  
365 of W1 Q5DOs obtained from the original method can be also underestimated during  
366 the 2008 SSW. For the amplitudes of E1 Q5DOs during the 2008 SSW, the original  
367 least-square fitting method may have an overestimation before the onset date and an  
368 underestimation after the onset date. As shown in Figure 4f, the positive and negative  
369 differences both have maximum amplitudes over 200 m in the mesosphere around the  
370 onset date.



371

372 Figure 5. Same as Figure 4 but for W2 and E2 Q5DOs during the 2013 SSW.

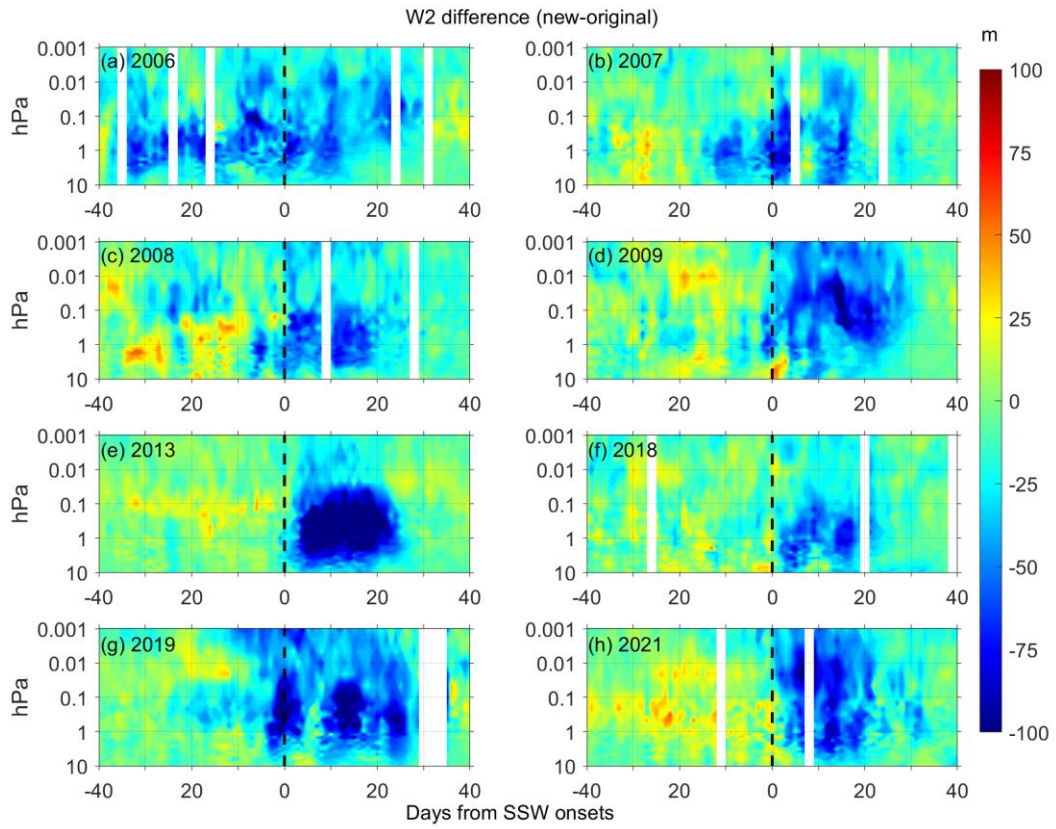
373 Figure 5 presents the same results as Figure 4 but for the amplitudes of W2 and  
 374 E2 Q5DOs during the 2013 SSW. As shown in Figure 5, strong enhancements of W2  
 375 Q5DOs and weak amplitudes of E2 Q5DOs after the 2013 SSW are captured by the  
 376 original least-square fitting method. However, results from the new method after the  
 377 onset of 2013 SSW suggest that based on the original least-square fitting method, the  
 378 amplitudes of W2 Q5DOs might be overestimated and the amplitudes of E2 Q5DOs  
 379 may be underestimated. The maximum positive and negative differences are both over  
 380 100 m. In order to understand the common differences between the two methods, we  
 381 calculate the differences during the eight SSWs and present the results in Figures 6, 7,  
 382 8, and 9 for the W1, W2, E1, and E2 components, respectively.



383

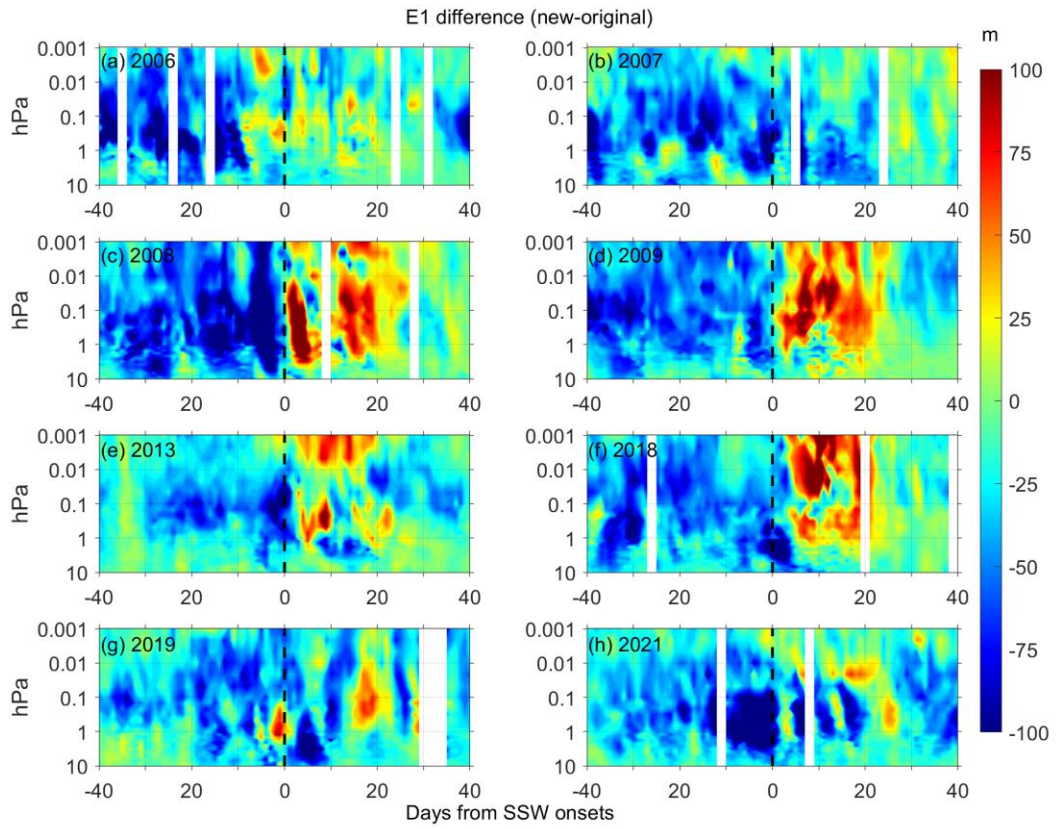
384 Figure 6. The differences in the fitted W1 Q5DO amplitudes between the new and

385 original methods during 8 major SSWs since 2006 (from a to h). Contour steps are 5 m.



386

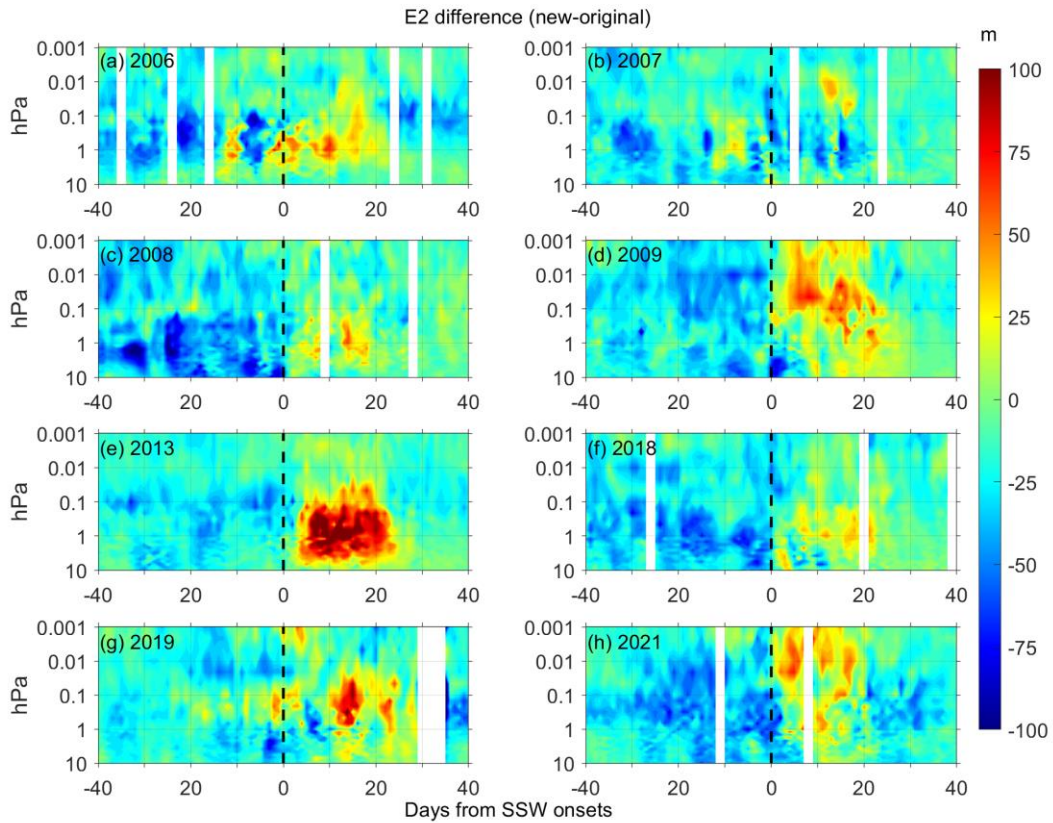
387 Figure 7. Same as Figure 6 but for the W2 component.



388

389 Figure 8. Same as Figure 6 but for the E1 component.





390

391 Figure 9. Same as Figure 6 but for the E2 component.

392 As shown in Figures 6 and 7, the difference in the fitted westward propagating  
 393 Q5DO amplitudes between the new and original methods are usually negative after the  
 394 SSW onsets, which suggests that the amplitudes of the westward propagating Q5DOs  
 395 might be overestimated by the original least-square fitting method after the SSW onsets.  
 396 However, the difference in the fitted eastward propagating Q5DO amplitudes between  
 397 the new and original methods (as shown in Figures 8 and 9) are usually positive after  
 398 the SSW onsets, which indicates that the amplitudes of the eastward propagating  
 399 Q5DOs might be underestimated by the original least-square fitting method after the  
 400 SSW onsets. Additionally, the E1 Q5DOs before the SSW onsets might be also  
 401 overestimated by the original least-square fitting method as seen in Figure 8. The

402 enhancements of traveling Q5DOs during SSWs reported in previous studies are  
403 usually westward propagating after the SSW onsets and eastward propagating before  
404 the SSW onsets (e.g., Gong et al., 2018; Yu et al., 2022). Thus, our analyses indicate  
405 that the previously-reported Q5DOs obtained by satellite measurements during SSWs  
406 might be contaminated by SPWs. The amplitudes of the enhancement of Q5DOs during  
407 SSWs might be overestimated. Additionally, the westward propagating Q5DOs before  
408 the SSW onsets and the eastward propagating Q5DOs after the SSW onsets might be  
409 underestimated by the original least-square fitting method. Therefore, in future studies  
410 of the activities of Q5DOs during SSWs based on satellite observations and reanalysis  
411 data, the variations of different wave components in Q5DOs have to be carefully  
412 derived by eliminating the effects of SPWs.

413       Generally, the TPWs, including the Q5DOs, dominate in the mesosphere and  
414 lower thermosphere, which are enhanced seasonally during winter and spring and  
415 largely control the winds and temperatures in the middle atmosphere (e.g., Gong et al.,  
416 2018, 2019; Pancheva et al., 2018; Yamazaki et al., 2020, 2021). The vertical and  
417 latitudinal propagation of the TPWs can also transport energies and lead to couplings  
418 on a global scale (e.g., Koushik et al., 2020; Ma et al., 2022). Thus, extracting the real  
419 amplitudes of the traveling waves is also important to reveal the characteristics in the  
420 mesosphere and the vertical couplings in the middle atmosphere. Some extremely  
421 strong TPWs are found to be related to the occurrence of SSWs, but their trigger  
422 mechanisms have not been fully understood (e.g., Ma et al., 2020; Yamazaki et al.,  
423 2021). However, the rapid and large change of the SPWs during SSWs can lead to

424 contaminations when deriving the real amplitudes of TPWs based on satellite  
425 observations or reanalysis data. The new method proposed in the present study can  
426 capture a more accurate variation in the amplitudes of TPWs than the old one. The new  
427 method is based on the examinations during SSWs due to the assumption that a rapid  
428 and large change in SPWs is usually observed during SSWs. Nevertheless, the new  
429 method can also be used to extract the amplitudes of TPWs in the mesosphere during  
430 other seasons and cases, such as the spring final warmings and other disturbances in  
431 stratospheric vortices. Based on the new method, the common feature of the TPWs  
432 revealed by satellite observations in the mesosphere and lower thermosphere can be  
433 reevaluated, and the trigger mechanism of the mesospheric TPWs during SSWs can be  
434 further understood.

## 435 **5. Summary and conclusions**

436 In the present study, a new fitting method is developed to derive the variations of  
437 traveling Q5DOs by inhibiting the effect of rapid and large changes in the amplitudes  
438 of SPWs. The effectiveness of the new method is demonstrated by both synthetic and  
439 observational data. According to the simulations, the new method can capture the  
440 variations of the amplitudes of traveling Q5DOs when large and rapid changes in SPWs  
441 are given. Based on the geopotential height data measured by MLS onboard the Aura  
442 satellite, we compare the difference of the traveling Q5DOs amplitudes between the  
443 original least-square fitting method and the new fitting method in the middle  
444 atmosphere during eight Arctic major SSWs from 2005 to 2021. Our results indicate

445 that the enhancements of traveling Q5DOs during SSWs reported in previous studies  
446 might be overestimated due to ignoring the effect of large rapid changes in SPWs.  
447 Besides, the amplitudes of westward propagating Q5DOs before the SSW onsets and  
448 the amplitudes of eastward propagating Q5DOs after the SSW onsets might be  
449 underestimated. Note that since the amplitudes of SPWs cannot be derived accurately  
450 due to the aliasing of Q5DOs, the contribution of the SPWs and Q5DOs during SSWs  
451 cannot be quantified in the present method. Our goal is to attenuate the effect of SPWs  
452 on the derivation of Q5DOs during SSWs. Future works are needed to examine the  
453 effectiveness of the new method by using traveling planetary oscillations with other  
454 periods, such as the quasi-10-day and quasi-16-day waves.

455

456 **Data availability.** The Aura/MLS geopotential height data can be downloaded through  
457 the Goddard Earth Sciences Data and Information Services Center via  
458 ([https://acdisc.gesdisc.eosdis.nasa.gov/data/Aura\\_MLS\\_Level2/ML2GPH.004/](https://acdisc.gesdisc.eosdis.nasa.gov/data/Aura_MLS_Level2/ML2GPH.004/)).

459

460 **Author contributions.** ZM and YG proposed the scientific ideas. QX and ZM  
461 contributed to data processing and simulation programming. ZM, YG, and SZ  
462 completed the analysis and manuscript. CH and KH discussed the results in the  
463 manuscript.

464

465 **Competing interests.** The authors declare that they have no conflict of interest.

466

467

468 **Acknowledgments.** We acknowledge the Goddard Earth Sciences Data and  
469 Information Services Center for providing the Aura/MLS geopotential height data.

470

471 **Financial support.** This study is supported by the Open Fund of Hubei Luojia  
472 Laboratory, the National Natural Science Foundation of China (through grants  
473 42104145, 41574142, and 42127805), the Fundamental Research Funds for the Central  
474 Universities 2042021kf0021, and the China Postdoctoral Science Foundation (through  
475 grants 2021M692465 and 2020TQ0230).

476

#### 477 **References**

478 Andrews, D. G., Holton, J. R., and Leovy, C. B.: Middle Atmosphere Dynamics, 1st  
479 ed., Academic Press, San Diego, Calif, 1987.

480 Baldwin, M. P., Ayarzagüena, B., Birner, T., Butchart, N., Butler, A. H., and Charlton-  
481 Perez, A. J.: Sudden stratospheric warmings. *Reviews of Geophysics*, 58,  
482 e2020RG000708. <https://doi.org/10.1029/2020RG000708>, 2021.

483 Butler, A. H., Seidel, D. J., Hardiman, S. C., Butchart, N., Birner, T., and Match, A.:  
484 Defining Sudden Stratospheric Warmings, *Bulletin of the American*  
485 *Meteorological Society*, 96(11), 1913-1928, [https://doi.org/10.1175/BAMS-D-13-](https://doi.org/10.1175/BAMS-D-13-00173.1)  
486 [00173.1](https://doi.org/10.1175/BAMS-D-13-00173.1), 2015.

487 Butler, A. H., Sjoberg, J. P., Seidel, D. J., and Rosenlof, K. H.: A sudden stratospheric

488 warming compendium. *Earth System Science Data*, 9, 63–76.  
489 <https://doi.org/10.5194/essd-9-63-2017>, 2017.

490 Charlton, A. J., and Polvani, L. M.: A new look at stratospheric sudden warmings. Part  
491 I: Climatology and modeling benchmarks. *J. Climate*, 20(3), 449–469.  
492 <https://doi.org/10.1175/JCLI3996.1>, 2007.

493 Choi, H., Kim, B. M., and Choi, W.: Type classification of sudden stratospheric  
494 warming based on pre- and postwarming periods. *Journal of Climate*, 32(8), 2349–  
495 2367. <https://doi.org/10.1175/JCLI-D-18-0223.1>, 2019

496 Davis, N.A., Richter, J.H., Glanville, A.A., Edwards, J., and LaJoie, E.: Limited surface  
497 impacts of the January 2021 sudden stratospheric warming. *Nature*  
498 *Communications*, 13, 1136. <https://doi.org/10.1038/s41467-022-28836-1>, 2022.

499 Domeisen, D. I. V., Butler, A. H., Charlton-Perez, A. J., Ayarzagüena, B., Baldwin, M.  
500 P., Dunn-Sigouin, E., Furtado, J. C., Garfinkel, C. I., Hitchcock, P., Karpechko, A.  
501 Yu., Kim, H., Knight, J., Lang, A. L., Lim, E., Marshall, A., Roff, G., Schwartz,  
502 C., Simpson, I. R., Son, S., Taguchi, M.: The role of the stratosphere in subseasonal  
503 to seasonal prediction: 2. Predictability arising from stratosphere-troposphere  
504 coupling. *Journal of Geophysical Research: Atmospheres*, 125, e2019JD030923.  
505 <https://doi.org/10.1029/2019JD030923>, 2020.

506 Gong, Y., Li, C., Ma, Z., Zhang, S., Zhou, Q., Huang, C., Huang, K., Li, G., Ning, B.:  
507 Study of the quasi-5-day wave in the MLT region by a meteor radar chain. *Journal*  
508 *of Geophysical Research: Atmospheres*, 123, 9474–9487.

509 <https://doi.org/10.1029/2018JD029355>, 2018.

510 Gong, Y., Wang, H., Ma, Z., Zhang, S., Zhou, Q., Huang, C., and Huang, K.: A statistical  
511 analysis of the propagating quasi 16-day waves at high latitudes and their response  
512 to sudden stratospheric warmings from 2005 to 2018. *Journal of Geophysical*  
513 *Research: Atmospheres*, 124, 12,617–12,630. <https://doi.org/10.1029/2019JD031482>,  
514 2019.

515 Harada, Y., and Hirooka, T.: Extraordinary features of the planetary wave propagation  
516 during the boreal winter 2013/2014 and the zonal wave number two predominance.  
517 *Journal of Geophysical Research: Atmospheres*, 122(21), 11374–11387.  
518 <https://doi.org/10.1002/2017JD027053>, 2017.

519 Harvey, V. L., Randall, C. E., Goncharenko, L., Becker, E., and France, J.: On the  
520 upward extension of the polar vortices into the mesosphere. *Journal of*  
521 *Geophysical Research: Atmospheres*, 123(17), 9171–9191.  
522 <https://doi.org/10.1029/2018JD028815>, 2018.

523 Huang, Y. Y., Zhang, S., Li, C. Y., Li, H. J., Huang, K., and Huang, C.: Annual and inter-  
524 annual variations in global 6.5DWs from 20–110 km during 2002–2016 observed  
525 by TIMED/SABER. *Journal of Geophysical Research: Space Physics*, 122, 8985–  
526 9002. <https://doi.org/10.1002/2017JA023886>, 2017.

527 King, A. D., Butler, A. H., Jucker, M., Earl, N. O., and Rudeva, I.: Observed  
528 relationships between sudden stratospheric warmings and European climate  
529 extremes. *Journal of Geophysical Research: Atmospheres*, 124(24), 13943–13961.

530 <https://doi.org/10.1029/2019JD030480>, 2019.

531 Koushik, N., Kumar, K. K., Ramkumar, G., Subrehmanyam, K. V., Kishore Kumar, G.,  
532 Hocking, W. K., He, M., Latteck, R.: Planetary waves in the mesosphere lower  
533 thermosphere during stratospheric sudden warming: Observations using a network  
534 of meteor radars from high to equatorial latitudes. *Climate Dynamics*, 54(9–10),  
535 4059–4074. <https://doi.org/10.1007/s00382-020-05214-5>, 2020.

536 Kozubek, M., Krizan, P., and Lastovicka, J.: Northern Hemisphere stratospheric winds  
537 in higher midlatitudes: longitudinal distribution and long-term trends. *Atmos.*  
538 *Chem. Phys.*, 15(4), 2203–2213. <https://doi.org/10.5194/acp-15-2203-2015>, 2015.

539 Lawrence, Z. D., and Manney, G. L.: Characterizing stratospheric polar vortex  
540 variability with computer vision techniques. *Journal of Geophysical Research:*  
541 *Atmospheres*, 123(3), 1510–1535., 2018.

542 Lin, J. T., Lin, C. H., Rajesh, P. K., Yue, J., Lin, C. Y., and Matsuo, T.: Local-time and  
543 vertical characteristics of quasi-6-day oscillation in the ionosphere during the 2019  
544 Antarctic sudden stratospheric warming. *Geophysical Research Letters*, 47.  
545 <https://doi.org/10.1029/2020GL090345>, 2020.

546 Livesey, N. J., Read, W. G., Wagner, P. A., Froidevaux, L., Lambert, A., Manney, G. L.,  
547 Millan Valle, L. F., Pumphrey, H. C., Santee, M. L., Schwartz, M. J., Wang, S.,  
548 Fuller, R. A., Jarnot, R. F., Knosp, B. W., and Martinez, E.: Earth Observing  
549 System (EOS) Aura Microwave Limb Sounder (MLS) Version 4.2x Level 2 data  
550 quality and description document, Tech. Rep. D-33509 Rev. A, JPL, 2015.



551 Liu, H. L., Talaat, E. R., Roble, R. G., Lieberman, R. S., Riggin, D. M., and Yee, J. H.:  
552 The 6.5-day wave and its seasonal variability in the middle and upper atmosphere.  
553 Journal of Geophysical Research, 109, D21112. <https://doi.org/10.1029/2004JD004795>,  
554 2004.

555 Liu, S.-M., Chen, Y.-H., Rao, J., Cao, C., Li, S.-Y., Ma, M.-H., and Wang, Y.-B.: Parallel  
556 Comparison of Major Sudden Stratospheric Warming Events in CESM1-WACCM  
557 and CESM2-WACCM. Atmosphere, 10, 679. <https://doi.org/10.3390/atmos10110679>,  
558 2019.

559 Longuet-Higgins, M. S.: The eigenfunctions of Laplace's tidal equations over a sphere,  
560 Philosophical Transactions of the Royal Society of London. 262, 511-607.  
561 doi:10.1098/rsta.1968.0003, 1968.

562 Lu, X., Wu, H., Oberheide, J., Liu, H.-L., and McInerney, J. M.: Latitudinal double-  
563 peak structure of stationary planetary wave 1 in the austral winter middle  
564 atmosphere and its possible generation mechanism. Journal of Geophysical  
565 Research: Atmospheres, 123, 11,551–11,568.  
566 <https://doi.org/10.1029/2018JD029172>, 2018.

567 Ma, Z., Gong, Y., Zhang, S., Zhou, Q., Huang, C., Huang, K., Luo, J., Yu, Y., Li, G.:  
568 Study of a quasi-4-day oscillation during the 2018/2019 SSW over Mohe, China.  
569 Journal of Geophysical Research: Space Physics, 125, e2019JA027687.  
570 <https://doi.org/10.1029/2019JA027687>, 2020.

571 Ma, Z., Gong, Y., Zhang, S., Xiao, Q., Xue, J., Huang, C., and Huang, K.:

572 Understanding the excitation of quasi-6-day waves in both hemispheres during the  
573 September 2019 Antarctic SSW. *Journal of Geophysical Research: Atmospheres*,  
574 127, e2021JD035984. <https://doi.org/10.1029/2021JD035984>, 2022.

575 Manney, G. L., Schwartz, M. J., Krüger, K., Santee, M. L., Pawson, S., Lee, J. N., Daffer,  
576 W. H., Fuller, R. A., and Livesey, N. J.: Aura Microwave Limb Sounder  
577 observations of dynamics and transport during the record breaking 2009 Arctic  
578 stratospheric major warming. *Geophys. Res. Lett.*, 36(12), L12815.  
579 <https://doi.org/10.1029/2009GL038586>, 2009.

580 Matsuno, T.: A dynamical model of the stratospheric sudden warming. *Journal of the*  
581 *Atmospheric Sciences*, 28, 1479–1494. [https://doi.org/10.1175/1520-](https://doi.org/10.1175/1520-0469(1971)028<1479:ADMOTS>2.0.CO;2)  
582 [0469\(1971\)028<1479:ADMOTS>2.0.CO;2](https://doi.org/10.1175/1520-0469(1971)028<1479:ADMOTS>2.0.CO;2), 1971.

583 Okui, H., Sato, K., Koshin, D., and Watanabe, S.: Formation of a mesospheric inversion  
584 layer and the subsequent elevated stratopause associated with the major  
585 stratospheric sudden warming in 2018/19. *Journal of Geophysical Research:*  
586 *Atmospheres*, 126, e2021JD034681. <https://doi.org/10.1029/2021JD034681>, 2021.

587 Pancheva, D., Mukhtarov, P., and Siskind, D. E.: The quasi-6-day waves in NOGAPS-  
588 ALPHA forecast model and their climatology in MLS/Aura measurements (2005-  
589 2014), *Journal of Atmospheric and Solar-Terrestrial Physics*, 181, 19-37,  
590 <https://doi.org/10.1016/j.jastp.2018.10.008>, 2018.

591 Qin, Y., Gu, S-Y., Teng, C-K-M., Dou, X-K., Yu, Y., and Li, N.: Comprehensive study  
592 of the climatology of the quasi-6-day wave in the MLT region based on aura/MLS

593 observations and SDWACCM-X simulations. Journal of Geophysical Research:  
594 Space Physics, 126, e2020JA028454. <https://doi.org/10.1029/2020JA028454>, 2021.

595 Rao, J., Ren, R., Chen, H., Liu, X., Yu, Y., Hu, J., and Zhou, Y.: Predictability of  
596 stratospheric sudden warmings in the Beijing Climate Center Forecast System  
597 with statistical error corrections. Journal of Geophysical Research:  
598 Atmospheres, 124, 8385–8400. <https://doi.org/10.1029/2019JD030900>, 2019.

599 Rao, J., Garfinkel, C. I., and White, I. P.: Predicting the downward and surface influence  
600 of the February 2018 and January 2019 sudden stratospheric warming events in  
601 subseasonal to seasonal (S2S) models. Journal of Geophysical Research:  
602 Atmospheres, 125, e2019JD031919. <https://doi.org/10.1029/2019JD031919>, 2020.

603 Rao, J., Ren, R., Chen, H., Yu, Y., and Zhou, Y.: The stratospheric sudden warming  
604 event in February 2018 and its prediction by a climate system model. Journal of  
605 Geophysical Research: Atmospheres, 123, 13,332–13,345.  
606 <https://doi.org/10.1029/2018JD028908>, 2018.

607 Rao, J., Garfinkel, C. I., Wu, T., Lu, Y., Lu, Q., and Liang, Z.: The January 2021 sudden  
608 stratospheric warming and its prediction in subseasonal to seasonal models.  
609 Journal of Geophysical Research: Atmospheres, 126, e2021JD035057.  
610 <https://doi.org/10.1029/2021JD035057>, 2021.

611 Rhodes, C. T., Limpasuvan, V., and Orsolini, Y. J.: Eastward-propagating planetary  
612 waves prior to the January 2009 sudden stratospheric warming. Journal of  
613 Geophysical Research: Atmospheres, 126, e2020JD033696.

614 <https://doi.org/10.1029/2020JD033696>, 2021.

615 Seviour, W. J. M., Mitchell, D. M., and Gray, L. J.: A practical method to identify  
616 displaced and split stratospheric polar vortex events. *Geophys. Res. Lett.*, 40(19),  
617 5268–5273. <https://doi.org/10.1002/grl.50927>, 2013.

618 Smith, A. K.: The origin of stationary planetary waves in the upper mesosphere. *Journal*  
619 *of the Atmospheric Sciences*, 60(24), 3033–3041. [https://doi.org/10.1175/1520-](https://doi.org/10.1175/1520-0469(2003)060<3033:TOOSPW>2.0.CO;2)  
620 [0469\(2003\)060<3033:TOOSPW>2.0.CO;2](https://doi.org/10.1175/1520-0469(2003)060<3033:TOOSPW>2.0.CO;2), 2003.

621 Tunbridge, V. M., Sandford, D. J., and Mitchell, N. J.: Zonal wave numbers of the  
622 summertime 2 day planetary wave observed in the mesosphere by EOS Aura  
623 Microwave Limb Sounder, *J. Geophys. Res.*, 116, D11103,  
624 doi:10.1029/2010JD014567, 2011.

625 Wang, J. C., Palo, S. E., Forbes, J. M., Marino, J., Moffat-Griffin, T., and Mitchell, N.  
626 J.: Unusual quasi 10-day planetary wave activity and the ionospheric response  
627 during the 2019 Southern Hemisphere sudden stratospheric warming. *Journal of*  
628 *Geophysical Research: Space Physics*, 126, e2021JA029286.  
629 <https://doi.org/10.1029/2021JA029286>, 2021.

630 Wang, Y., Shulga, V., Milinevsky, G., Patoka, A., Evtushevsky, O., Klekociuk, A., Han,  
631 W., Grytsai, A., Shulga, D., Myshenko, V., and Antyufeyev, O.: Winter 2018 major  
632 sudden stratospheric warming impact on midlatitude mesosphere from microwave  
633 radiometer measurements, *Atmos. Chem. Phys.*, 19, 10303–10317,  
634 <https://doi.org/10.5194/acp-19-10303-2019>, 2019.

635 White, I. P., Garfinkel, C. I., Cohen, J., Jucker, M., and Rao, J.: The impact of split and  
636 displacement sudden stratospheric warmings on the troposphere. *Journal of*  
637 *Geophysical Research: Atmospheres*, 126, e2020JD033989.  
638 <https://doi.org/10.1029/2020JD033989>, 2021.

639 Wright, C. J., Hall, R. J., Banyard, T. P., Hindley, N. P., Krisch, I., Mitchell, D. M., and  
640 Seviour, W. J. M.: Dynamical and surface impacts of the January 2021 sudden  
641 stratospheric warming in novel Aeolus wind observations, MLS and ERA5,  
642 *Weather Clim. Dynam.*, 2, 1283–1301, <https://doi.org/10.5194/wcd-2-1283-2021>,  
643 2021.

644 Wu, D. L., Hays, P. B., and Skinner, W. R.: A least-squares method for spectral-analysis  
645 of space-time series, *J. Atmos. Sci.*, 52, 3501–3511, [https://doi.org/10.1175/1520-](https://doi.org/10.1175/1520-0469(1995)052<3501:ALSMFS>2.0.CO;2)  
646 [0469\(1995\)052<3501:ALSMFS>2.0.CO;2](https://doi.org/10.1175/1520-0469(1995)052<3501:ALSMFS>2.0.CO;2), 1995.

647 Xiong, J., Wan, W., Ding, F., Liu, L., Hu, L., and Yan, C.: Two day wave traveling  
648 westward with wave number 1 during the sudden stratospheric warming in January  
649 2017. *Journal of Geophysical Research: Space Physics*, 123, 3005–3013.  
650 <https://doi.org/10.1002/2017JA02517>, 2018.

651 Xu, J., Smith, A. K., Wang, W., Jiang, G., Yuan, W., Gao, H., Yue, J., Funke, B., López-  
652 Puertas, M., Russell, I. I. I., and M, J.: An observational and theoretical study of  
653 the longitudinal variation in neutral temperature induced by aurora heating in the  
654 lower thermosphere. *Journal of Geophysical Research: Space Physics*, 118, 7410–  
655 7425, 2013.

656 Yamazaki, Y., and Matthias, V.: Large-amplitude quasi-10-day waves in the middle  
657 atmosphere during final warmings. *Journal of Geophysical Research:*  
658 *Atmospheres*, 124, 9874–9892. <https://doi.org/10.1029/2019JD030634>, 2019.

659 Yamazaki, Y., Matthias, V., Miyoshi, Y., Stolle, C., Siddiqui, T., Kervalishvili, G.,  
660 Laštovička, J., Kozubek, M., Ward, W., Themens, D. R., Kristoffersen, S., Alken,  
661 P.: September 2019 Antarctic sudden stratospheric warming: Quasi-6-day wave  
662 burst and ionospheric effects. *Geophysical Research Letters*, 47, e2019GL086577.  
663 <https://doi.org/10.1029/2019GL086577>, 2020.

664 Yamazaki, Y., Matthias, V., and Miyoshi, Y.: Quasi-4-day wave: Atmospheric  
665 manifestation of the first symmetric Rossby normal mode of zonal wavenumber 2.  
666 *Journal of Geophysical Research: Atmospheres*, 126, e2021JD034855.  
667 <https://doi.org/10.1029/2021JD034855>, 2021.

668 Yu, F. R., Huang, K. M., Zhang, S. D., Huang, C. M., and Gong, Y.: Observations of  
669 eastward propagating quasi 6-day waves from the troposphere to the lower  
670 thermosphere during SSWs in early 2016. *Journal of Geophysical Research:*  
671 *Atmospheres*, 127, e2021JD036017, <https://doi.org/10.1029/2021JD036017>, 2022.

672  
673